ELSEVIER

Journal of Nuclear Materials 299 (2001) 227–234

journal of nuclear materials

www.elsevier.com/locate/jnucmat

Determination of the defect creation mechanism in the mono-silicated fluoroapatite. Disorder modeling under repository conditions

Stéphane Soulet [a,b], Joëlle Carpéna [b], Jacques Chaumont [a,*], Jean-Claude Krupa [c], Marie-Odile Ruault [a]

[a] *Centre de Spectrométrie Nucléaire et de Spectrométrie de Masse, CNRS-IN2P3, Bat 104-108, 91405 Orsay Campus, France*
[b] *CEA-Cadarache, DCC/DESD/SEP, 13108 Saint-Paul-lez-Durance, France*
[c] *Institut de Physique Nucléaire, CNRS-IN2P3, 91406 Orsay cedex, France*

Received 14 December 2000; accepted 5 September 2001

Abstract

Amorphization resulting from α-decay events can strongly reduce the chemical durability of nuclear waste matrices. The creation rate of defects produced by α recoils in mono-silicated fluoroapatite was determined using a transmission electron microscope (TEM) on line with an ion implanter and compared to previous results obtained in fully phosphated fluoroapatite. In both materials, the defect creation is controlled at room temperature, by the amorphization process directly in the cascade. Furthermore, it has been shown previously that in mono-silicated fluoroapatite, the disorder recovery proceeds mainly via α-annealing. Taking into account our already published data and new results on the defect creation in the mono-silicated fluoroapatite, we have modeled the amorphization level evolution versus time under repository conditions. The main conclusion is the following: thanks to α-annealing, mono-silicated fluoroapatite loaded with ^{244}Cm, will maintain a disorder at a level low enough to prevent the total amorphization of the host lattice during the long-term disposal.

PACS: 23.60.+e; 61.72Cc; 61.80.Az

1. Introduction

Many studies are devoted to stabilization or immobilization of high-level radioactive waste. One of the strategies usually considered is the incorporation of radionuclides into stable crystalline phases. These host matrices must have a good thermal and chemical stability in an irradiating environment. Indeed, the chemical durability of crystalline actinide waste form can be strongly reduced when α-decay events generate enough disorder to induce a crystalline to amorphous phase transition. This phase transformation may enhance the ceramic water dissolution and may produce a large swelling giving rise to cracks or even a fragmentation of the waste form increasing the leached area [1]. Thus, for a long-term disposal in crystalline waste forms, an important point to consider is the atomic disorder level evolution versus time.

Natural minerals have already provided first way of assessing the long-term performance of potential host phases in high-level irradiating environment. Some of these natural minerals having incorporated significant amounts of actinides; their studies have provided data to estimate the possible behavior of synthesized waste forms as far as the resistance to radiation and the chemical durability over long periods of time are concerned. For example, crystalline minerals with an apatitic structure were found in Ouzzal Mole in Hoggar (Algeria) [2], though having experienced radiation doses ranging from 1×10^{19}–3×10^{19} α-events/g (Table 1). These doses are higher than typical apatite amorphiza-

* Corresponding author. Tel.: +33-1 69 15 52 88; fax: 33-1 69 15 52 68.
E-mail address: chaumont@csnsm.in2p3.fr (J. Chaumont).

0022-3115/01/$ - see front matter
PII: S0022-3115(01)00697-3

Table 1
Material state as a function of cumulated α-decay event dose in 2.1×10^9 years-old apatite natural analogs of chemical formula: $Ca_{10-x}(REE, U, Th)_x(SiO_4)_x(PO_4)_{6-x}(F, Cl)_2$

Sample	Ca	Si	P	F	U (ppm)	Th (ppm)	α events/g	State
INH604	8.90	0.67	5.28	1.54	315	6000	1.16×10^{19}	Crystalline
INH187	8.29	1.12	4.82	1.60	150	9000	1.48×10^{19}	Crystalline
INH604	7.70	1.76	4.15	1.56	350	14 000	2.40×10^{19}	Metamict
INH604	6.20	3.44	2.70	1.22	300	18 000	2.97×10^{19}	Metamict
INH603	4.56	5.41	0.64	1.06	280	9000	1.59×10^{19}	Metamict
INH603	4.15	5.76	0.69	1.30	350	14 000	2.40×10^{19}	Metamict

Ouzzal Mole (Algeria) [2].

tion doses which are for example close to 10^{19} α-events/g for a fully silicated oxyapatite [1,3] and to 5×10^{18} α-events/g for a fully phosphated fluoroapatite [4,5]. Based on these geochemical observations [3,6,7], the possibility of using synthetic analogs of natural apatites as nuclear waste disposal matrices has been evaluated [8–13]. Among them, the mono-silicated fluoroapatite has provided strong evidence to be a potential waste form [6,7,12]. This mineral is always found crystalline despite having experienced thermal events, severe irradiating environment and aqueous lixiviations both in neutral or alkaline media [2,6]. In the same environmental conditions, the more silicated apatites are all found in metamict state (Table 1). Then, it is clear that in mono-silicated fluoroapatite, defect annealing mechanisms have operated over geological periods. In this respect, previous experiments have shown that in fully phosphated fluoroapatite ($Ca_{10}(PO_4)_6F_2$) [14–16] and in the mono-silicated fluoroapatite ($Ca_9Nd(SiO_4)(PO_4)_5F_2$) [16] an important defect recovery process is induced by the electronic energy loss of emitted α-particles. In both matrices, α-annealing is much more efficient than thermal annealing [15,17] and the latter can even be considered as a negligible recovery process except for very low α-decay rates and for geological environments where temperatures over 100 °C could be encountered.

The modeling of the disorder level evolution versus time in actinide host lattice implies the creation and annealing rate measurements of the disorder produced by every α-recoils as a function of temperature. In fully phosphated fluoroapatite, we have already shown that at a disposal temperature of 60 °C, the disorder induced by α-recoils will reach an equilibrium level at 17% of damage and this level does not depend on the dose rate [18,19]. Therefore, the actinide content is not a critical parameter for $Ca_{10}(PO_4)_6F_2$ waste form regarding amorphization. However fully phosphated fluoroapatite cannot accommodate a large amount of actinide without changing its chemical composition. Since natural analogs have clearly identified the mono-silicated fluoroapatite as a potential waste form [6,7,12] and since its chemical composition can hold larger amounts of actinides, the present study is focused on this host matrix. The α-annealing rate of defects having already been measured in mono-silicated fluoroapatite [16], the experimental part of this study is devoted to the determination of the defect creation rate. Then, using the differential equation that controls the disorder evolution as a function of time [17], it was possible to evaluate, through a numerical simulation, the effect due to the incorporation of ^{244}Cm in mono-silicated fluoroapatite versus disposal time.

2. Experimental techniques

The creation mechanism of defects due to α-recoils has been studied using a 120 kV transmission electron microscope (TEM) on line [20] with the 190 kV IRMA ion implanter [21] allowing in situ irradiation. 320 keV Pb-ions were used to simulate at room temperature the 100 keV α-recoils. This energy has been chosen to increase the disordered layer thickness without modifying the nature of the defect and thus to improve the signal over noise ratio in the amorphization curve measurement. The Pb-ion current was set at 0.05 $\mu A/cm^2$ to keep the ion-beam heating effect at a negligible level. Irradiation has been performed by steps of 10^{13} Pb/cm^2. After each irradiation step, the disorder level was measured using the TEM–selected area electron diffraction technique (SAED) [22].

The TEM samples were cut from mono-silicated fluoroapatite material obtained by reactive sintering at 1500 °C for 6 h (grain size of 3–10 μm) [23,24]. They were shaped in discs of 3 mm in diameter and 2 mm in thickness. The discs were thinned down to a 200 μm thickness and one face was carefully polished with diamond powder suspensions down to a grain size of 0.25 μm. The other face was bowl shaped and polished down to a 5–10 μm thickness in the center. Then, an argon ion mill was used, at room temperature, to thin the sample up to perforation and finally, a 6 nm conductive carbon layer was evaporated on the plane face. At last, every sample was thermally annealed at 500 °C during 2 h.

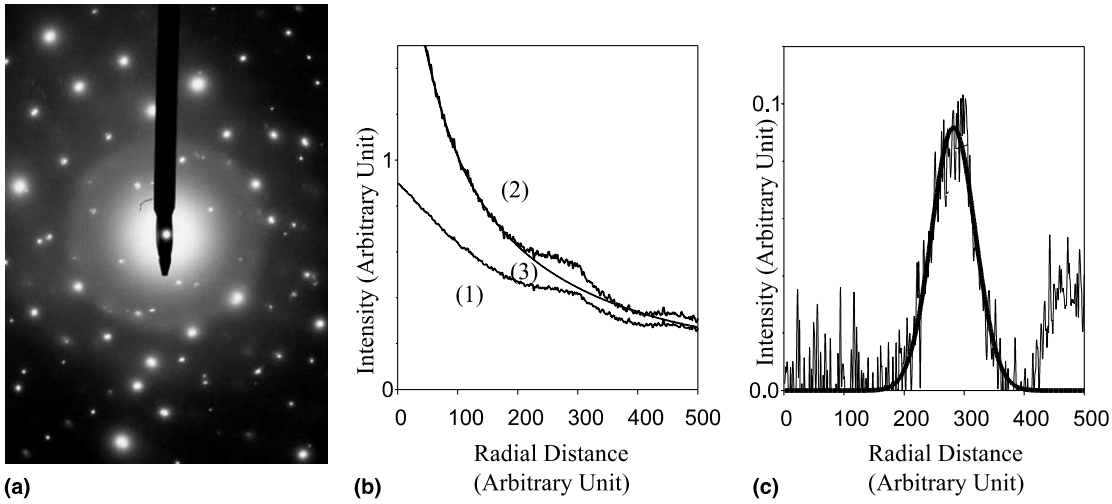

Fig. 1. (a) Diffraction pattern after 3×10^{13} Pb/cm^2 implantation. The diffuse ring due to the electron diffraction on the amorphous zones and the diffraction maximum due to the crystalline remaining part are displayed. (b) Typical diffuse ring intensity profile: (1) as measured, (2) after correction for photographic plate non-linearity, (3) background fitting using the sum of two exponentials and a constant term [16]. (c) Intensity distribution after background subtraction fitted by a gaussian distribution to determine its maximum.

Electron diffraction patterns performed on virgin crystalline samples shows a zone axis diagram very often accompanied by one or two weaker secondary zone axis produced by electron diffraction on close grains. When samples are partially amorphized by irradiation, a diffuse halo is superimposed on the crystalline diagram (Fig. 1(a)). Since the intensity of this diffuse halo is proportional to the amorphous amount [16,25], its evolution as a function of Pb-ion fluence provides the amorphization curve of the mono-silicated fluoroapatite lattice.

Four conditions must be fulfilled to be able to compare the different SAED patterns obtained during in situ experiments and to plot the measured intensities on the same curve [16].

(i) It is necessary to work with the same crystalline orientation which had to be far from any low index axis to avoid large variations of the electron fraction that produces the diffuse halo [25].

(ii) Since the sample has an inhomogeneous thickness, every measurement must be performed with the same electron-beam spot size at the same sample position in order to keep constant the primary crystalline fraction of the selected area.

(iii) An electron beam current as low as 0.5 nA should be spread over a 50 μm^2 sample area (1 mA/cm^2) to lower the defect annealing by the analyzing beam [26,27]. Under this condition, and considering that the time necessary to come back on a given sample area to take a new picture is approximately one minute, one can estimate that the analyzing electrons annealing is less than 1% of defects that are present.

(iv) The diffraction patterns should be registered on photographic plates with always the same exposure electron dose. To take into account the electron-beam current variation, its intensity is measured precisely with a Faraday cup before each SAED measurement.

All the shots corresponding to a given area on the sample must be developed simultaneously to prevent any perturbations due to the developer temperature and age [25]. They are digitized to measure the intensity of the diffuse halo. The darkening of each picture is then measured along four different radial directions chosen free of crystal diffraction spots to take into account the non-homogeneity of the diffuse halo intensity. Each recorded intensity profile is corrected to account for the non-linear response of the photographic plate [16] (Fig. 1(b)). The diffuse halo appears over a background produced by the scattered electrons, that varies rapidly with the radial distance (Fig. 1). Therefore, a rather large zone on both side of the diffuse halo has to be considered to determine the background profile and the amount to be subtracted (Fig. 1(b)). The average value of the intensity maxima recorded on the four radial directions is used to determine the disorder level after each irradiation (Fig. 1(c)).

3. Experimental results

The measured diffuse halo intensity as a function of Pb-ion fluence gives the evolution of the mean disorder amount. Since the thickness of at least a part of the investigated area is certainly larger than the lead ion

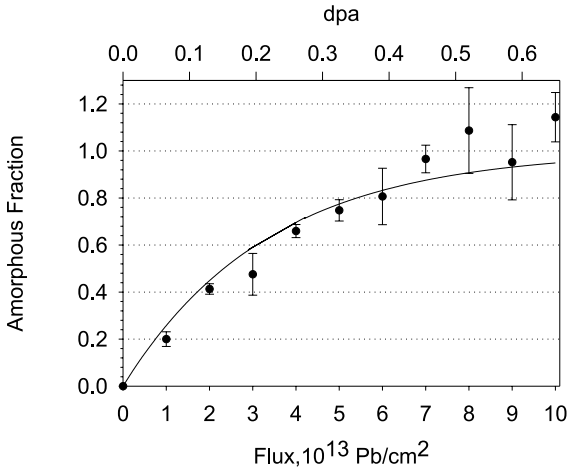

Fig. 2. Amorphization curve of $Ca_{10}(PO_4)_6F_2$ as a function of lead ion fluence and corresponding dpa number. The solid line is obtained using Eq. (1).

stopping range, the amorphization dose cannot be determined accurately. However, one can notice that the experimental points reported in Fig. 2 as a function of Pb-ion fluence can be well fitted by Eq. (1).

$$y = 1 - \exp(-V\Phi/R), \tag{1}$$

where y is the disorder fraction when there is no defect post-cascade annealing, Φ is the ion fluence, V is the mean amorphized volume per ion impact and R is the mean amorphized thickness. Eq. (1) fit provides a V/R ratio equal to $(3.0 \pm 0.3) \times 10^{-14}$ cm^2.

4. Defect creation mechanism

The fit in Fig. 2 shows that the mono-silicated fluoroapatite amorphization is controlled by the direct-impact model [28,29]. This amorphization mechanism has been already reported for a ^{244}Cm loaded silicate apatite host: $Ca_2Nd_8(SiO_4)_6O_2$ [1,3] and for fluoroapatite $Ca_{10}(PO_4)_6F_2$ irradiated by 320 keV-Pb ion [18,19]. Then, the amorphization of apatites based on silicate and phosphate anions can be described by the same model. In this case, every ion or α-recoil creates a small amorphous volume in the virgin part of the crystal. SRIM calculation [30], for mono-silicated fluoroapatite irradiated by 320 keV Pb-ions, gives a mean amorphized thickness, R, equal to 73 nm. Therefore, the amorphous volume created by each lead ion is $V = (2.2 \pm 0.3) \times 10^{-19}$ cm^3. Our previous study on fully phosphated fluoroapatite has provided an amorphous volume equal to $(3.3 \pm 0.4) \times 10^{-19}$ cm^3 per ion [18,19]. Consequently, the amorphization dose for the mono-silicated fluoroapatite is larger than for the fully phosphated fluoroapatite at room temperature. This enhancement of the amorphization dose with the SiO_4 grouping content is in agreement with the critical amorphization doses measured for $Ca_{10}(PO_4)_6F_2$ and $Ca_2Nd_8(SiO_4)_6O_2$ under 1.5 MeV Kr-ion irradiation [4,5] at room temperature.

From our experimental results and SRIM calculation using a displacement threshold energy of 25 eV, the Pb-ion amorphization doses can be expressed through the number of displacements per atom (dpa). A 0.65 dpa value is calculated for the mono-silicated fluoroapatite. For the fully phosphated fluoroapatite, we obtain 0.45 dpa [18,19] which is in agreement with the value of 0.5 dpa given by Ouchani et al. [14]. However, these values are larger than the 0.3 dpa, calculated with the same displacement threshold energy from 1.5 MeV Kr-ion irradiation experiment in $Ca_{10}(PO_4)_6F_2$ [4,5]. In the latter study, amorphization is induced not only by the nuclear stopping power of Kr-ion but, more probably, also by the 1.44 keV/nm electronic stopping power of Kr-ions. Indeed, this value is very similar to the electronic stopping power of 5 MeV B-ions that, in spite of a negligible nuclear stopping power [14,15], amorphizes the fully phosphated fluoroapatite with only 10^{15} B/cm^2. Since 0.3 dpa in $Ca_{10}(PO_4)_6F_2$ are induced by 3×10^{14} cm^2 (1.5 MeV Kr-ions), the Kr-ion electronic losses may reduce the amorphization dose by a factor of about 1.5.

5. Disorder evolution under repository conditions

5.1. Disorder modeling

The evolution of the relative damaged fraction in the apatite host phase can be expressed as a balance between defect creation and recovery rates. As was shown above, the silicated-apatite amorphization occurs via the direct-impact model and the differential equation established by Chaumont et al. [17] can be used to calculate the evolution of the disorder level, y, as a function of time in an actinide loaded mono-silicated fluoroapatite host lattice.

$$\mathrm{d}y = V_0(T)[1-y]\,\mathrm{d}D - y[(c(T)E_\alpha/2)\,\mathrm{d}D + R(T)\,\mathrm{d}t]. \tag{2}$$

This equation contains:

(i) The disorder creation term, $V_0(T)$, that is the mean disordered volume produced by a α-recoil nucleus at temperature T; the crystalline fraction $(1-y)$ and $\mathrm{d}D$, the dose increment.

(ii) The α-annealing term, $c(T)$, that corresponds to the volume recovery per eV deposited by a α-particle having an energy E_α. When α-annealing operates, the disordered fraction, y, decreases according to a mono-exponential law as a function of the α-fluence [14]. It means that the annealing effect measured by $\mathrm{d}y$, is always proportional to y

and only the energy deposited into the amorphous zones is efficient for the defect recovery.

(iii) The defect thermal annealing term, $R(T)$, that depends on temperature: $R(T) = F\exp(-E_a/kT)$ with, F, the jump frequency and, E_a, the activation energy. This thermal annealing term is proportional to the surface area of the crystalline to amorphous interface. This area cannot be precisely calculated since the shape of individual disordered volume is not known. However, one can consider that after a certain time, a more or less steady size distribution will probably be established and consequently, we can assume that the thermal annealing term is proportional to the disordered volume y as a first approximation.

The differential equation (2) can only be partially solved using the initial conditions: $y = 0$ and $D = 0$ at $t = 0$ (see Appendix A). It gives rise to Eq. (3) where the amorphous fraction, y, appears as a function of the cumulative dose, D

$$y = y_{eq}[1 - (R(T)I(t) + 1)\exp(-(V_0(T) + c(T)E_\alpha/2)D - R(T)t)] \quad \text{with}$$

$$y_{eq} = V_0(T)/(V_0(T) + c(T)E_\alpha/2 \quad \text{and}$$

$$I(t) = \int_0^t \exp[(V_0(T) + c(T)E_\alpha/2)D + R(T)u]\,du. \qquad (3)$$

This equation was already solved for the fully phosphated fluoroapatite [17–19]. In this work concerning the mono-silicated fluoroapatite matrix loaded with 10 wt% of ^{244}Cm as an example, Eq. (3) is numerically solved using different parameters given below:

(i) ^{244}Cm ($t_{1/2} = 18.1$ years, $E_\alpha = 5.8$ MeV) is a radionuclide which decays successively toward ^{240}Pu ($t_{1/2} = 6570$ years, $E_\alpha = 5.18$ MeV) and ^{236}U ($t_{1/2} = 2.4 \times 10^7$ years) which is considered as stable in the present simulation.

(ii) The disordered volume $V_0(T)$ produced by a 95 keV recoiling ^{240}Pu atom is $V_0(25\ ^\circ\text{C}) = 7.9 \times 10^{-20}$ cm^3. This volume has been calculated from the disordered volume created by 320 keV Pb-ion in mono-silicated fluoroapatite, assuming that both volumes are proportional to the respective number of displaced atoms obtained from SRIM calculations [30].

(iii) The volume recovery per eV or the α-annealing efficiency has been previously determined: $c(35\ ^\circ\text{C}) = 2.5 \times 10^{-26}$ cm^3/eV for the mono-silicated fluoroapatite [16] but the defect thermal annealing term, $R(T)$, has not yet been evaluated in this host lattice. However, as the thermal annealing efficiency is very low, we can use, as a first approximation, data which were previously obtained on fully phosphated fluoroapatite [15]. These data will not introduce a large error in calculations.

5.2. Temperature effect on the defect creation and annealing rate: $V_0(T)$, $c(T)$ and $R(T)$

During disposal time, the waste form temperature will be higher than the ambient conditions where $V_0(T)$ and $c(T)$ have been measured. This temperature is not yet well defined. So, two different temperatures (60 and 100 °C) were used in the calculation of the disorder evolution in the mono-silicated fluoroapatite loaded with actinides.

Since the behavior versus temperature of this host lattice has not yet been studied, the thermal evolution of $V_0(T)$, $c(T)$ and $R(T)$ parameters has been assumed to be identical to those obtained for the fully phosphated fluoroapatite. Under this assumption the extrapolation of our results at 60 and 100 °C give:

(i) an amorphous volume equal to $V_0(60\ ^\circ\text{C}) = 6.6 \times 10^{-20}$ cm^3 and $V_0(100\ ^\circ\text{C}) = 4.6 \times 10^{-20}$ cm^3 [4,5,18], (ii) a volume recovery per eV of $c(60\ ^\circ\text{C}) = 3.8 \times 10^{-26}$ cm^3/eV and $c(100\ ^\circ\text{C}) = 5.5 \times 10^{-26}$ cm^3/eV [15], and finally (iii) the thermal annealing term $R(T)$ is equal to 7.5×10^{-8} yr^{-1} and 2.3×10^{-5} yr^{-1} at 60 and 100 °C, respectively [17]. These disorder thermal recovery rates correspond to a defect lifetime of 9 million years and 30 000 years, respectively.

5.3. Disorder evaluation in mono-silicated fluoroapatite

From these data and Eq. (3), the disorder evolution versus time in the mono-silicated fluoroapatite at both temperatures can be calculated. The results plotted in Fig. 3 show that at 60 and 100 °C the disorder level increases rapidly to reach an equilibrium regime between the defect creation and the defect annealing rates. The difference in y_{eq}, 40% and 25%, respectively for both temperatures, is due to the enhancement of the α-annealing efficiency and the reduction of V_0 with temperature. The equilibrium level remains constant versus time in spite of dose rate variation until the defect creation rate becomes negligible (about 5×10^5 years with 10wt% of ^{244}Cm) and the thermal annealing operates. At 100 °C, this decrease occurs even before 5×10^5 years due to the increase of the thermal annealing efficiency. In turn, the time necessary to reach the plateau is dose rate dependent. Therefore, as for the fully phosphated fluoroapatite [18,19], the actinide content is not a critical parameter regarding amorphization. However, at a temperature of 60 °C, the equilibrium disorder level of 40% inside the matrix is too high. Indeed, at the surface the corresponding disorder level will be about 55% since the α-flux is reduced by a factor 2 [17]. If aqueous lixiviation occurs, this high value will increase the actinide release. Subsequently, the equilibrium will be destroyed and the matrix will undergo amorphization. To overcome this difficulty, an increase of the repository temperature can

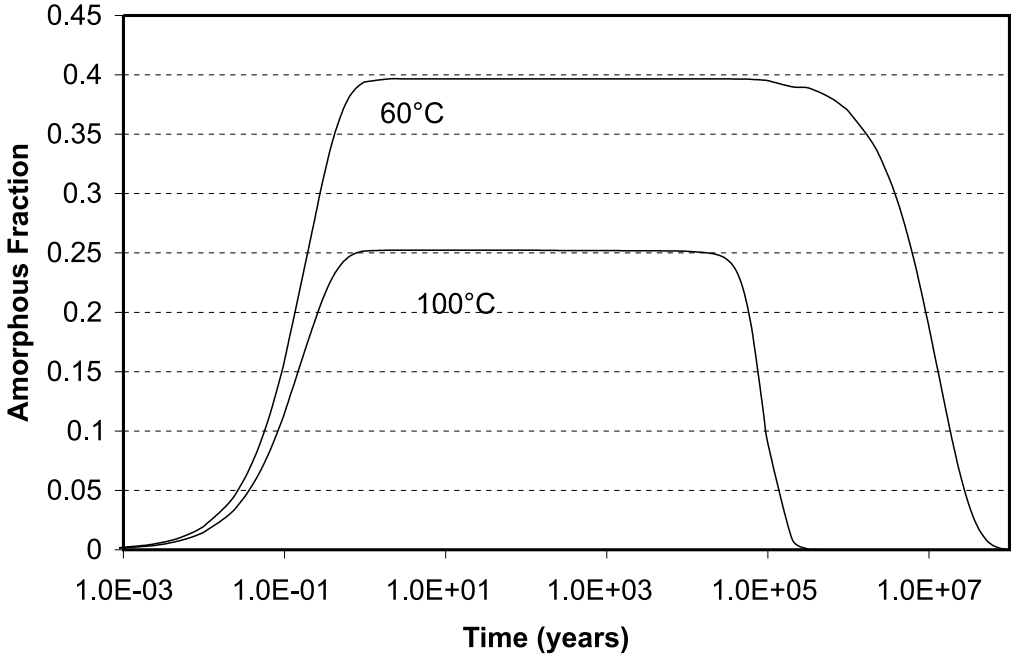

Fig. 3. Disorder level evolution as a function of time in a mono-silicated fluoroapatite matrix loaded with 10 wt% of ^{244}Cm at 60 °C and at 100 °C.

be considered as well as a reduction of the silicate grouping concentration to get a better α-annealing efficiency [16].

There is no significant variation of the disorder level when ^{244}Cm is substituted for its daughter ^{240}Pu having a lower α-energy because the recoiling atom energy is reduced in the same proportion.

6. Conclusion

The defect creation study in mono-silicated fluoroapatite confirms that the direct-impact amorphization is the dominant process for a large range of apatite compositions. This amorphization mechanism has already been reported for ^{244}Cm loaded silicated apatite: $Ca_2Nd_8(SiO_4)_6O_2$ [1,3] and in our previous study on fully phosphated $Ca_{10}(PO_4)_6F_2$ irradiated by 320 keV-Pb ion [18,19] simulating α-recoils.

Under repository conditions, the behavior of the mono-silicated fluoroapatite loaded with 10 wt% of actinide has been evaluated. Our calculation has shown that in this particular apatite composition, the disorder will be maintained at a level low enough not only to prevent amorphization but also to avoid a large increase of the leach rate if the waste form temperature is set around 100 °C. More accurate data on the defect creation and annealing are still needed to validate the behavior of this potential actinide host phase. For instance, the low thermal annealing efficiency as well as the defect creation and the α-annealing rates should be measured as a function of temperature.

In the proposed following chemical formula of a potential apatitic phase to host actinide: $Ca_{10-x}Nd_{x-y}An_y(SiO_4)_x(PO_4)_{6-x}F_2$ with $y < x$ and $x \leqslant 1$ [10], the actinide concentration is not a critical parameter since the maximum disorder level is not dependent upon the dose rate. Furthermore, it is known that the introduction of SiO_4 anionic grouping into this structure influences the water dissolution resistance. Then the x coefficient value must be determined more accurately to get the best compromise between the chemical resistance and the α-annealing efficiency to minimize the actinide release in underground water.

Acknowledgements

We gratefully acknowledge the assistance of the technical staff of the SEMIRAMIS team. We are indebted to O. Kaitasov and S. Gautrot who performed the Pb-ion implantation, as well as to L. Boyer and J.L. Lacout who initiated the synthesis of phospho-silicated fluoroapatite. This work is a part of the PhD studies of S.S. who is supported by the French Commissariat à l'Energie Atomique.

Appendix A

The differential equation (Eq. (2)) can be partially solved by standard methods using the initial conditions: $y = 0$ and $D = 0$ at $t = 0$. In a first step, we have solved Eq. (2) without a second member (wsm) i.e.

$$\frac{dy}{dt} + y\left[\frac{dD}{dt}(V_0(T) + c(T)E_\alpha/2) + R(T)\right] = 0. \quad (A.1)$$

Solution of Eq. (A.1) is obtained with K constant, D being the cumulative α-decay dose

$$y_{wsm} = K\exp[-(V_0(T) + c(T)E_\alpha/2)D - R(T)t]. \quad (A.2)$$

The solution of Eq. (2) is then given by

$$y = y_{wsm} + y_{part}, \quad (A.3)$$

where y_{part} is a particular solution of Eq. (2) defined by

$$y_{part} = K(t)\exp[-(V_0(T) + c(T)E_\alpha/2)D - R(T)t]. \quad (A.4)$$

This equation can be inserted into Eq. (2) in order to obtain the following expression of $K(t)$:

$$K(t) = y_{eq}\int_{u=0}^{t}(V_0(T) + c(T)E_\alpha/2)\frac{dD}{dt}\exp[(V_0(T) + c(T)E_\alpha/2)D + R(T)u]\,du \quad (A.5)$$

with $y_{eq} = V_0(T)/(V_0(T) + c(T)E_\alpha/2)$ which is a constant.

Eq. (A.5) can be written as

$$K(t) = y_{eq}[\exp[(V_0(T) + c(T)E_\alpha/2)D + R(T)t] - R(T)I(t)]$$

with

$$I(t) = \int_{u=0}^{t}\exp[(V_0(T) + c(T)E_\alpha/2)D + R(T)u]\,du. \quad (A.6)$$

The combination of (A.2)–(A.4) gives the expression of the amorphous fraction y

$$y = (K + K(t))\exp[-(V_0(T) + c(T)E_\alpha/2)D - R(T)t]. \quad (A.7)$$

This equation can be written as follows using Eq. (A.6)

$$y = y_{eq} + [K - y_{eq}R(T)I(t)]\exp(-(V_0(T) + c(T)E_\alpha/2)D - R(T)t). \quad (A.8)$$

Using the initial condition, $y = 0$ and $D = 0$ at $t = 0$, the constant K is easily found to be equal to $-y_{eq}$. Then, the solution of the differential equation (Eq. (3)) is

$$y = y_{eq}[1 - (1 + R(T)I(t))\exp(-(V_0(T) + c(T)E_\alpha/2)D - R(T)t)]. \quad (A.9)$$

References

[1] W.J. Weber, R.C. Ewing, C.R.A. Catlow, T. Diaz de La Rubia, L.W. Hobbs, C. Kinoshita, Hj. Matzke, A.T. Motta, M.A. Nastasi, E.H.K. Salje, E.R. Vance, S.J. Zinkle, J. Mater. Res. 13 (1998) 1434.
[2] J. Carpena, J.R. Kienast, K. Ouzegane, C. Jehanno, Geol. Soc. Amer. Bull. 100 (1998) 1237.
[3] W.J. Weber, R.C. Ewing, A. Meldrum, J. Nucl. Mater. 250 (1997) 147.
[4] R.C. Ewing, L.M. Wang, W.J. Weber, Mater. Res. Soc. Proc. 373 (1995) 347.
[5] L.M. Wang, M. Cameron, W.J. Weber, K.D. Crowley, R.C. Ewing, in: P.W. Brown, B. Constantz (Eds.), Hydroxyapatite and Related Materials, CRC, Boca Raton, FL, 1994, p. 243.
[6] J. Carpena, in: P. Van Den Hante, F.D. Eorte (Eds.), Advances in Fission Track Geochronology, Kluwer Academic, Dordrecht, 1998, p. 81.
[7] V. Sere, PhD thesis, University Paris VII, 1995, 226p.
[8] J. Carpena, J.L. Lacout, French Patent 93 08676 (1993) .
[9] R.C. Ewing, W.J. Weber, W. Lutze, in: E.R. Merz, C.E. Walter (Eds.), Disposal of Weapons Plutonium, Kluwer Academic, Netherlands, 1996, 65p.
[10] J. Carpena, L.Boyer, J.L. Lacout, French Patent 98 11334 (1998).
[11] J. Carpena, J.L. Lacout, Act. Chimi. 2 (1997) 3.
[12] C.V. Sere, J.R. Kienast, Proceedings 'Migration 95', St-Malo, France, 1995.
[13] R. Bros, J. Carpena, V. Sere, A. Beltritti, Radiochim. Acta 74 (1996) 277.
[14] S. Ouchani, J.-C. Dran, J. Chaumont, Nucl. Instrum. Meth. B 132 (1997) 447.
[15] S. Ouchani, PhD thesis, University of Paris XI, 1997.
[16] S. Soulet, J. Carpena, J. Chaumont, O. Kaitasov, M.O. Ruault, J.C. Krupa, Nucl. Instrum. Meth. B (2001) in press.
[17] J. Chaumont, S. Soulet, J.C. Krupa, J. Carpena, submitted.
[18] S. Soulet, J. Carpena, J. Chaumont, J.C. Krupa, M.O. Ruault, J. Nucl. Mater. 289 (2001) 194.
[19] S. Soulet, PhD thesis, University of Paris XI, 2000.
[20] M.O. Ruault, J. Chaumont, H. Bernas, Nucl. Instrum. Meth. B 209/210 (1983) 351.
[21] J. Chaumont, F. Lalu, M. Salomé, A.M. Lamoise, H. Bernas, Nucl. Instrum. Meth. B 9 (1981) 344.
[22] A. Traverse, M.O. Ruault, L. Mendoza-Zelis, M. Schack, H. Bernas, J. Chaumont, in: S.T. Picraux, W.J. Choyke (Eds.), Metastable Materials Formation by Ion Implantation, Elsevier, New York, 1984.
[23] L. Boyer, J. Carpena, J.L. Lacout, Solid State Ionics 95 (1996) 121.
[24] L. Boyer, PhD thesis, INP-Toulouse, 1999.
[25] M. Schack, PhD thesis, University of Paris XI, 1984.
[26] A. Meldrum, L.A. Boatner, R.C. Ewing, MRS Proc. 439 (1996).

[27] A. Meldrum, L.A. Boatner, R.C. Ewing, J. Mater. Res. 12 (7) (1998) 1816.
[28] J.F. Gibbons, Proc. IEEE 60 (1972) 1062.
[29] G. Carter, R. Webb, Radiat. Eff. Lett. 43 (1979) 19.
[30] J.F. Ziegler, J.P. Biersack, D.J. Marwick, SRIM-2000, The Stopping and Range of Ions in Matters, IBM Corporation, New York, 1999.